Band edge States, Intrinsic Defects and Dopants in Monolayer HfS_2 and SnS_2

Haichang Lu[1], Yuzheng Guo[2], John Robertson[1]*

[1]Department of Engineering, Cambridge University, Cambridge CB2 1PZ, United Kingdom
[2]College of Engineering, Swansea University, Swansea SA1 8EN, United Kingdom

Although monolayer HfS_2 and SnS_2 do not have a direct band gap like MoS_2, they have much higher carrier mobilities. Their band offsets are favorable for use with WSe_2 in tunnel field effect transistors. Here, we study the effective masses, intrinsic defects and substitutional dopants of these dichalcogenides. We find that HfS_2 has surprisingly small effective masses for a compound that might appear partly ionic. The S vacancy in HfS_2 is found to be a shallow donor while that in SnS_2 is a deep donor. Substitutional dopants at the S site are found to be shallow. This contrasts with MoS_2 where donors and acceptors are not always shallow or with black phosphorus where dopants can reconstruct into deep non-doping configurations. It is pointed out that HfS_2 is a more favorable than MoS_2 for semiconductor processing because it has the more convenient CVD precursors developed for growing HfO_2.

The open-shell transition metal dichalcogenides (TMDs) such as MoS_2 have been intensively researched as important two-dimensional semiconductors. Their band gap changes from indirect in the bulk to direct for the monolayer case [1]. The relatively small dielectric screening in the monolayer case means that complex exciton behavior becomes important even for relative small band gaps [2]. Carriers can be manipulated between the degenerate valley states in valleytronics [3]. TMDs are also interesting as photo- and molecular sensors. On the other hand, for purely electronic devices, we can consider other layered semiconductors which might have a carrier higher mobility.

One proposed electronic device is the heterojunction tunnel field effect transistor (TFET). In this case, the continued scaling of transistors for computation creates a need for very low power switches, in particular switches with a steep subthreshold slope below the thermionic limit of 60 mV/decade of a normal field effect transistor [4-7]. We note that TFETs operating in the subthreshold regime are also very sensitive sensor amplifiers [8]. TFETs would normally be built using heterojunctions of two lattice-matched III-V semiconductors with a staggered or broken-gap band alignment. However, the lattice-matching condition is not always met and this leads to interfacial mismatch defects which degrade switching performance. An alternative is to use stacked layer heterojunctions of two TMDs. TMDs offer a wide range of band gaps and band offsets [9-12], and, due to their van der Waals inter-layer bonding, no lattice matching condition is needed to avoid dangling bond-type defects. Considering the band offsets of the various 2D semiconductors, a suitable choice is a p-type compound with d^2 configuration such as WSe_2 paired with an n-type d^0 compound such as HfS_2 or SnS_2 [9-12]. WSe_2 has a suitably high ionization potential whereas HfS_2 and SnS_2 have suitably deep electron affinities. SnS_2 and HfS_2 have s,p-like band edges and so, like black phosphorus, they have a higher phonon limited mobility of order 1000 $cm^2/V.s$ and lower effective masses than MoS_2 [13,14].

The electronic properties of HfS_2 or SnS_2 are much less studied than the standard TMDs such as MoS_2 or WSe_2, It is particularly important to understand the intrinsic defects and anion vacancies of these materials because these defects can cause Fermi level pinning at the contacts [15-19], which

causes a large contact resistance. This is a principle cause of the under-performance of 2D devices [20,21]. Thus, this paper investigates the band edge states, the intrinsic defects and the substitutional dopants of these chalcogenides.

The calculations are carried out with the CASTEP plane-wave density functional theory (DFT) code [22,23] for periodic supercell models of the Hf/Sn disulfides. Ultra-soft pseudopotentials are used and the Perdew-Burke-Ernzerhof (PBE) form of the generalized gradient approximation (GGA) is used for the electronic exchange-correlation functional for geometry relaxation. The HSE (Heyd-Scuseria-Ernzerhof) [24] hybrid functional is used to calculate the band structures and the heats of formation. The HSE parameters α and ω are set to 0.2 as in HSE06 to give band gaps consistent with experimental values. The screened exchange (SX) method [23] is also used for heats of formation, for comparison. Spin-orbital coupling is not included. The plane wave cut-off energy is set as 260 eV. All atomic structures are relaxed to a residual force of less than 10^{-5} eV/atom. Van der Waals corrections [25,26] are included for bulk structures.

For the 2D Hf/Sn disulfide system, a convergence test finds that a vacuum layer thickness of 20Å in the z direction is enough to converge the formation energy of S vacancy, and that 5x5 supercells in the x,y direction are enough to allow us to neglect periodic images. The transition states of intrinsic defects are corrected using the Lany and Zunger scheme [27]. The formation energy of each charge state are given by

$$H_q(E_F,\mu) = [E_q - E_H] + q(E_V + \Delta E_F) + \Sigma_\alpha n_\alpha (\mu_\alpha^0 + \Delta\mu_\alpha)$$

where q is the charge on the system, E_q is the energy of charged system with a defect, E_H is the energy of charged defect-free system. E_V is the valence band maximum (VBM) and E_F is the Fermi level with the respect to VBM. n_α is the number of atoms of species α, μ_α is the relative chemical potential of element α. We note that the first two terms are equal to the difference between the total energy of charged defect system and total energy of the neutral defect-free system.

HfS_2 and SnS_2 each have the 2H structure with an octahedral metal site. The lattice constant of HfS_2 is calculated to be 3.68Å in PBE, which is 1.4% more than experimental value of 3.62Å [28]. The lattice constant of SnS_2 is calculated to be 3.74Å, which is 2.9% more than experimental value of 3.64Å [28].

We then calculate the chemical potential for the S-rich and S-poor limits. In the S-rich limit, chemical potential of S is set to 0 eV. In the S-poor limit for HfS_2, the S chemical potential is set to the Hf-HfS_2 equilibrium, from the heat of formation of HfS_2 (Table 1). This is calculated to be -5.10 eV or 2.55 eV/S atom in HSE, compared to -2.58 eV/S atom experimentally [29]. For SnS_2, the monovalent sulfide SnS exists between SnS_2 and Sn metal [29-33], so the range of S chemical potential for SnS_2 is from 0 to -0.50 eV/ S atom, or 0 to -0.50 eV experimentally [31-33].

The band structures of bulk SnS_2 and HfS_2 have been studied for some time [34-38]. Fig. 1 and 2 show the band structures of monolayer and bulk HfS_2 and SnS_2 calculated with the HSE functional. There is an indirect band gap in both monolayer and bulk forms, which is different to the case of MoS_2 and other d^2 transition metal dichalcogenides. The band gap is from Γ to M for the monolayer and from Γ to L for the bulk.

Table 2 compares the band gaps of these two materials calculated in PBE and HSE and the experimental band gaps for the bulk form [39]. Generally speaking, HSE06 corrects any under-estimation of the band gap of PBE.

The calculated Bader charges are +0.34 for Hf in HfS_2 and +0.3 for Sn in SnS_2 showing that the bonding is relatively non-polar in these compounds despite the formal ionic charges often used to describe their bonding.

Table 3 shows the calculated effective masses for SnS_2 and HfS_2. The non-polar bonding (only 8% ionic for HfS_2) explains the relatively dispersed band structures and the small effective masses of these compounds. Our hole masses of SnS_2 differ slightly from those of Gonzalez [38].

Fig 3 shows the calculated band alignments with respect to the vacuum level [12]. These were calculated using supercells containing a monolayer of sulphide and 20Å of vacuum. This shows that WSe_2 has a type II band alignment with monolayer HfS_2 and SnS_2 in HSE as desired for a vertically stacked heterojunction TFET.

We now consider the geometries and formation energies of the intrinsic defects. Fig.4(a) shows the vacancy configuration. When the S atom is removed, the Hf or Sn and S atoms around the vacancy all move slightly away from vacancy center, compared to the defect-free configuration. Fig. 4(b) shows the defect formation energy as a function of Fermi energy E_F in the S-poor limit and the charge transition states. Here, the energies are plotted with respect to the charge neutrality level (CNL) [40] to enable both compounds to be plotted in a single diagram. For HfS_2, the -2 state is stable across all of the gap and with no state in the gap. The transition state lies at the bottom of the conduction band, so the vacancy is a shallow donor. For SnS_2, there is a transition level for –2 to +2 in the upper gap at +0.3 eV above the CNL. This vacancy is a deep donor.

Fig. 5(a) shows the partial density of states (PDOS) of the neutral defect state. For HfS_2, there is a peak in the PDOS at the conduction band edge with E_F lying at the conduction band edge. For SnS_2, transition state +2/-2 lies in the upper gap, above a defect band, consistent with Fig 4. The tendency to lose two electrons is the same for HfS_2 except that Fig. 5(b) now has two PDOS peaks for the +2/0 and 0/-2 states.

The behavior of the S vacancy in the d^0 compound HfS_2 differs from that of the S vacancy in the d^2 compounds MoS_2 where the neutral vacancy has a donor state in the upper band gap and a filled state at the valence band edge [18,41].

The sulfur interstitial configuration is shown in Fig. 4(c). This adatom configuration is found in many layered compounds. The S-S bond is calculated to be 1.99Å in HfS_2 and 1.98Å in SnS_2. The S-S bond is longer than the double bond and shorter than S-S single bond in S_8. Fig. 4(d) shows the formation energies and transition state of this defect in HSE06. PBE gives three transition states in the gap +2/+1, +1/0, 0/-2, while HSE shows two defect states, +1/0, 0/-2. The +1/0 state lies in the middle of gap, and the 0/-2 state lies at the conduction band edge. The orbitals for +2/+1 and +1/0 states are shown in Fig. 4(c). The +2/+1 orbitals consist of degenerate p_x and p_y states of the S adatom. The +1/0 orbitals have the same two orbitals but more located on underlying S atom. HSE gives a similar result, but only the +1/0 state is found, lying 0.7 eV below the CBM. This behavior is similar to the S interstitial in monolayer MoS_2 [41]. (It should be noted that the S interlayer interstitial in bulk SnS_2 is slightly different, where it tries to bond to both layers [32,33].)

The Hf interstitial has two configurations in monolayer HfS_2, as seen in Figs. 4(e,g). (The Sn interstitial in SnS_2 is similar.) One configuration has two Hf atoms stacked vertically on top of each other called the ‘onsite’ or ‘split interstitial’. The other configuration places the extra Hf atom outside the layer at the hollow center of three S atoms in the ‘hollow interstitial’. Their formation energies are shown as a function of E_F in Fig 4(d).

For the split interstitial, the adjacent S atoms move away from defect center to allow space for the extra metal atom. The two metal atoms are equivalent for the split interstitial. These atoms form in-plane bonds with the three adjacent S atoms. The system is symmetric in the z direction. There are 4 valence electrons on Hf and Sn, two of which form three bonds with S. The other electron forms a Hf-Hf or Sn-Sn bond. There is one unpaired electron left, which can easily ionise. Hence, the +2 charge system dominates. The two electrons in Hf-Hf or Sn-Sn bond ionize if E_F moves across the transition energy. Both HfS_2 and SnS_2 have a similar mid-gap +4/+2 transition state. A mid-gap peak is seen at 0.4eV in Fig 4(c,d), where the transition state is located.

The symmetry in the z direction is lost for the 'hollow interstitial'. Three adjacent S atoms distort outward and out of the plane. There are two unpaired electrons in the extra Hf/Sn atom. Fig. 4(h) shows the transition states. The HfS_2 has a +4/+2 transition near the VBM and SnS_2 has nearly no transition state. Overall, plotting the formation energy of both interstitials across the band gap, the hollow site is the lowest for HfS_2 and the lowest for SnS_2 except very close to the valence band.

The metal vacancy states have also been calculated. Their formation energies for the neutral defects for the S-rich (metal-poor) limit are 4.38 eV and 5.31 eV for HfS_2 and SnS_2, respectively. These formation energies are much higher than for the other defects. Therefore, we conclude that Hf and Sn vacancies are not very important.

We have also calculated the formation energies in PBE. While PBE underestimates band gap and the formation energy, it usually gives the right location of transition state with respect to the CNL. As Hf/SnS_2 is used for the n-type layer of the TFET, so E_F will lie close to the CBM. The S vacancy, interstitial and Hf/Sn interstitial each have a positive formation energy near the CBM, which means that they will not form spontaneously.

Fig 6 shows the substitutional doping states at the S site. The Br donor is calculated to be a shallow state, with a transition state near the respective band edge. The As acceptor is deeper, but still reasonably close to the VBM. This is very desirable if these compounds are to be used for a TFET. The fact that neither of the dopant sites reconstructs into a non-doping configuration explains why these sites are basically shallow, unlike the case of dopants in black phosphorus [42].

We summarise the situation of these two compounds for use as a TFET. Their band offsets are as desired. SnS_2 has a low effective mass and is bipolar, with shallow donors and acceptors. Its main disadvantage is that it has only a small range of S chemical potential for which it is stable, which is important for growth by chemical vapor deposition (CVD). Superficially, HfS_2 is more ionic than SnS_2 so might be expected to have higher effective masses. However, in practice, its bonding is *not* very polar, and its effective masses are still low. Its big advantage is that it is the only stable sulfide of Hf, stable over a large range of S chemical potential, and with a large heat of formation. It has the great advantage that Hf CVD precursors are highly developed from the use of HfO_2 as a high K oxide in microelectronics, whereas precursors for MoS_2 like $Mo(CO)_6$ are less volatile and poisonous. The disadvantage of HfS_2 is that the S vacancy is a shallow donor. This will require CVD of HfS_2 to be carried out in S-rich conditions to increase the S vacancy formation energy and decrease its concentration. This might result in the formation of S interstitial adatoms, as already seen by Aretouli et al [43]. Such adatoms may affect the quality of epitaxial growth. This would require careful control of S activity. Thus, HfS_2 is competing with InSe for use in TFETs. InSe has suitable band offsets, bipolar doping ability and suitably behaved intrinsic defects [44], but may be less convenient CVD.

Finally, we have calculated the exfoliation energies for these compounds using the method of Bjorkman et al [45] and the Tkatchenko-Scheffler [26] scheme for van der Waals interactions. Our values in Table 4 are similar to those found previously [45].

In conclusion, HfS_2 and SnS_2 are indirect band gap semiconductors but otherwise very suitable for electronic devices because of their low effective masses and higher mobility than MoS_2. The high heat of formation makes it convenient for CVD. The main intrinsic defects in Hf/SnS_2 are the S vacancy, S interstitial and Hf/Sn interstitial. The S vacancy forms a gap state in SnS_2 and a shallow donor in HfS_2. The S interstitial is a low formation adatom. Substitutional dopants give reasonably shallow states. Therefore, both HfS_2 and SnS_2 can be considered as building blocks for TFETs.

We thank EPSRC grant EP/P005152/1 and CSC for support.

REFERENCES

1. K. F. Mak, C. Lee, J. Hone, J. Shan, T. F. Heinz, Phys Rev Lett **105,** 136805 (2010).
2. J S Rose, S F Wu, H Y Yu, N J Ghimiro, A M Jons, G Aivarau, J Q Yan, D G Mandrus, D Xiao, W Yao, X D Xu, Nat Comm **4** 1474 (2013)
3. K F Mai, K He, J Shan, T F Heinz, Nature Nano **7** 494 (2012)
4. T. N. Theis, P M Solomon, Science **327,** 1600 (2010)
5. D. Sarkar, X.J. Xie, W. Liu, W. Cao, J.H. Kang, Y.J.Gong, S. Kraemer, P. Ajayan, K. Banerjee, Nature **526,** 91 (2015)
6. T Roy, M Tosun, M Hettick, G H Ahn, C M Hu, A Javey, Appl. Phys Lett **108** 083111 (2016)
7. S. Das, A. Prakash, R. Salazar, J. Appenzeller, ACS Nano **8,** 1681 (2014).
8. D Sarkar, W Liu, X Xie, A C Anselmo, S Mitragotri, K Banerjee, ACS Nano 8 3992 (2014)
9. C. Gong, H. J. Zhang, W. H. Wang, L. Colombo, R. M. Wallace, K. J. Cho, Appl Phys Lett **103**, 053513 (2013)
10. J. Kang, S. Tongay, J. Zhou, J.B. Li, J.Q. Wu, Appl Phys Lett **102,** 012111 (2013).
11. Y.F. Liang, S.T. Huang, R. Soklaski, L. Yang, Appl Phys Lett **103** 042106 (2013).
12. Y. Guo, J. Robertson, Appl Phys Lett **108,** 233104 (2016)
13. Y. Huang, E. Sutter, J. T. Sadowski, M. Cotlet, O. L. A. Monti, D. A. Racke, M. R. Neupane, D. Wickramaratne, R. K. Lake, B. A. Parkinson, P. Sutter, ACS Nano ***8***, 10743.(2014)
14. T Kanazawa, T Amemiya, A Ishikawa, V Upadhyaya, Y Miyamoto, Sci. Reports 6 22277 (2016)
15. S McDonnell, R Addou, C Brule, R M Wallace, C L Hinkle, ACS Nano **8** 2880 (2014)
16. C M Smyth, R Addou, S McDonnell, C L Hinkle, R M Wallace, J Phys Chem C **120** 14719 (2016)
17. Y Guo, D Liu, J Robertson, ACS Appl Mater Interfaces **7**, 25709 (2015)
18. D Liu, Y Guo, L Fang, J Robertson, Appl. Phys. Lett.**103**, 183113 (2013)
19. Y Guo, D Liu, J Robertson, App Phys Lett **106** 173106 (2015)
20. S. Das, A. Prakash, R. Salazar, J. Appenzeller, ACS Nano **8,** 1681 (2014).
21. A. Allain, J. H. Kang, K. Banerjee, A. Kis, Nat Mater **14,** 1195 (2015)
22. S. J. Clark, M. D. Segall, C. J. Pickard, P. J. Hasnip, M. J. Probert, K. Refson, M. C. Payne, Z Kristallogr **220,** 567 (2005)
23. S. J. Clark, J. Robertson, Phys Rev B **82,** 085208 (2010)
24. J Heyd, G E Scuseria, M Ernzerhof, J. Chem. Phys, **118** 8207 (2003)
25. S. Grimme, J Comput Chem **27,** 1787 (2006)
26. A. Tkatchenko and M. Scheffler, Phys. Rev. Lett. **102,** 073005 (2009)
27. S. Lany and A. Zunger, Phys. Rev. B **78**, 235104 (2008)
28. D L Greenaway, D L Nitsche, J Phys Chem Solids 26 1445 (1965)
29. http://www.nims.go.jp/softionics/wadahr/HfpSe.htm
30. O Kubaschewski, C B Alcock, Metallurgical Thermochemistry (Pergamon,Oxford, 1979)
31. L A Burton, D Colombara, R D Abellon, F C Grozema, L M Peter, T J Savenjie, G Dennier, A L Walsh, Chem Mater **25** 4908 (2013)
32. T J Whittles, L A Burton, J M Skelton, A Walsh, T D Veal, V R Dhanak, Chem Mater **28** 3718 (2016)
33. Y Kumagai, L A Burton, A Walsh, F Oba, Phys Rev Appl **6** 014009 (2016)
34. C Y Fong, M L Cohen, Phys Rev B 5 3095 (1972); J Robertson, J Phys C **12** 4753 (1979)
35. L F Mattheiss, Phys Rev B **8** 3719 (1973)
36. H Jiang, J Chem Phys **134** 204705 (2011)
37. F.A. Rasmussen, K.S. Thygesen, J Phys Chem C **119,** 13169 (2015)
38. J M Gonzalez, I I Oleynik, Phys Rev B **94** 125443 (2016)
39. R. Schlaf, O. Lang, C. Pettenkofer, W. Jaegermann, J App Phys **8***5*, 2732 (1999).
40. J Robertson, J Vac Sci Technol B 18 2760 (2000); J Robertson, App Surf Sci 190 2 (2002)
41. J Y Noh, H Kim, Y S Kim, Phys Rev B **89** 205417 (2014)
42. Y. Guo, J. Robertson, Sci Rep **5** 14165 (2015)
43. K.E. Aretouli, P. Tsipas, D. Tsoutsou, J. Marquez-Velasco, E Xenogiannopoulou, S.A. Giamini, E. Vassalou, N Kelaidis, A Dimoulas, Appl Phys Lett **106** 143105 (2015)

44. Y Guo, J Robertson, Phys Rev Mater **1** 014004 (2017)
45. T Bjorkman, A Gulans, A V Krasheninnkov, R M Nieminen, Phys Rev Lett 108 235502 (2012)

Table 1. Heats of formation [29,30].

	eV/mole
MoS_2	-3.04
HfS_2	-5.16
SnS_2	-1.53
SnS	-1.13

Table 2 Calculated Band gaps of HfS_2 and SnS_2 compared to experimental values [13,39,12]. ML = monolayer, CNL = charge neutrality level.

Band gaps (eV)	HfS_2		SnS_2	
	ML	bulk	ML	Bulk
PBE	0.98		1.50	
HSE	2.05	1.68	2.40	2.30
SX	2.12	1.95	2.68	2.0
Exp		1.98		2.18
CNL (ML)	1.11		1.55	

Table 3 Effective masses for monolayer. e=electron, h=hole, x and y are along ΓK and ΓM respectively.

	HfS_2	SnS_2
m_ex	0.25	0.27
m_ey	1.85	0.72
m_hx	0.48	1.2
m_hy	0.49	2.8

Table 4 Exfoliation energies (meV/Å^2).

HfS_2	SnS_2
22.2	10.2

Figure Captions

1. Band structures for the monolayers

2. Band structures for the bulk compounds

3. Calculated band offsets for stacked monolayers of HfS_2, SnS_2 and WSe_2.

4. Geometries and defect formation energies vs Fermi energies for (a,b) S vacancy, (c,d) S adatom interstitial, (e) geometry split interstitial and (g) hollow interstitial for HfS_2 and SnS_2. (f,h) compare the formation energies for the metal interstitial defect in (f) HfS_2 and (h) SnS_2 alone.

5. Partial density of states for the defect-free monolayer, S vacancy, S interstitial, metal split-interstitial and hollow interstitial, all in their neutral states, for HfS_2 and SnS_2.

6. (a,b) Geometries of substitutional Br and As dopants at the S site in HfS_2, and (c) formation energy vs. Fermi energy.

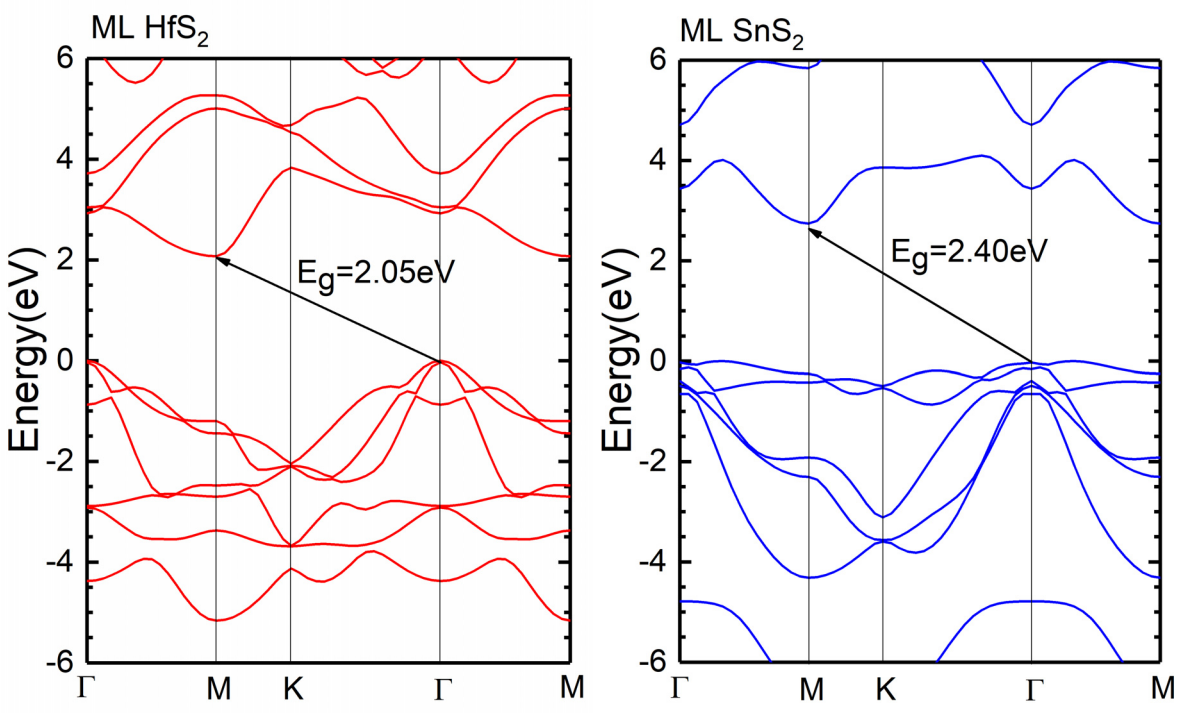
ML HfS2
Energy(eV)
6
4
2
0
-2
-4
-6
Eg=2.05eV
Γ
M
K
Γ
M
ML SnS2
Energy(eV)
Eg=2.40eV
Γ
M
K
Γ
M

Fig. 1.

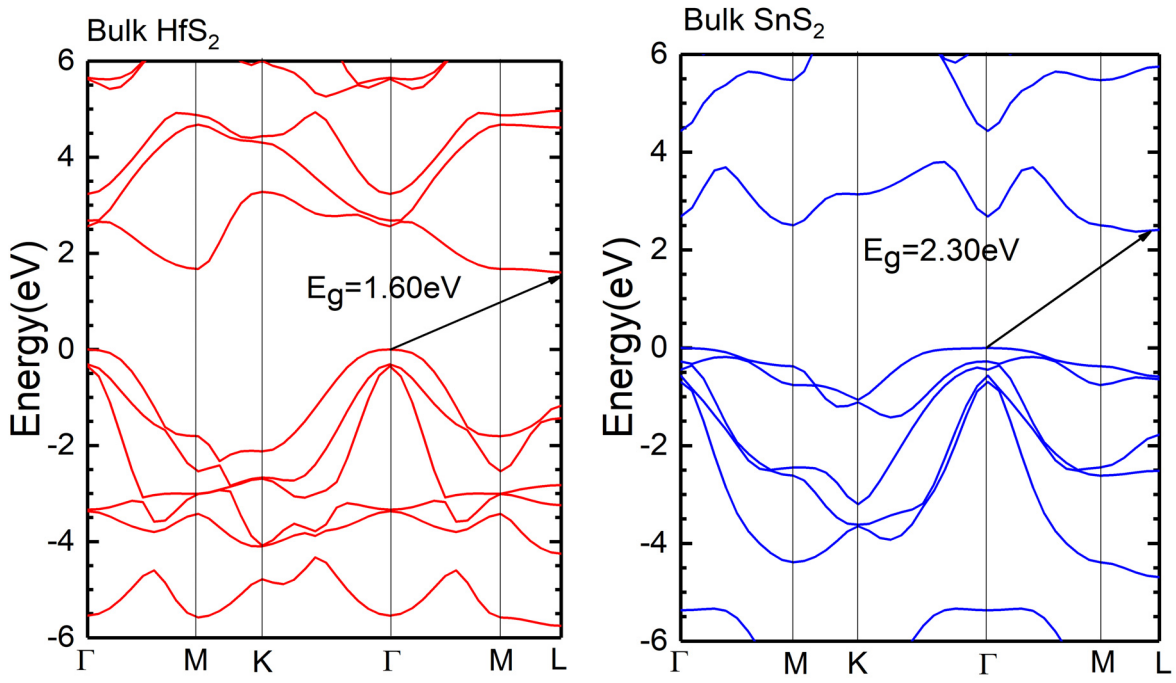
Bulk HfS_2
Energy(eV)
6
4
2
0
-2
-4
-6
E_g=1.60eV
Γ
M
K
Γ
M
L
Bulk SnS_2
Energy(eV)
E_g=2.30eV
Γ
M
K
Γ
M
L

Fig. 2.

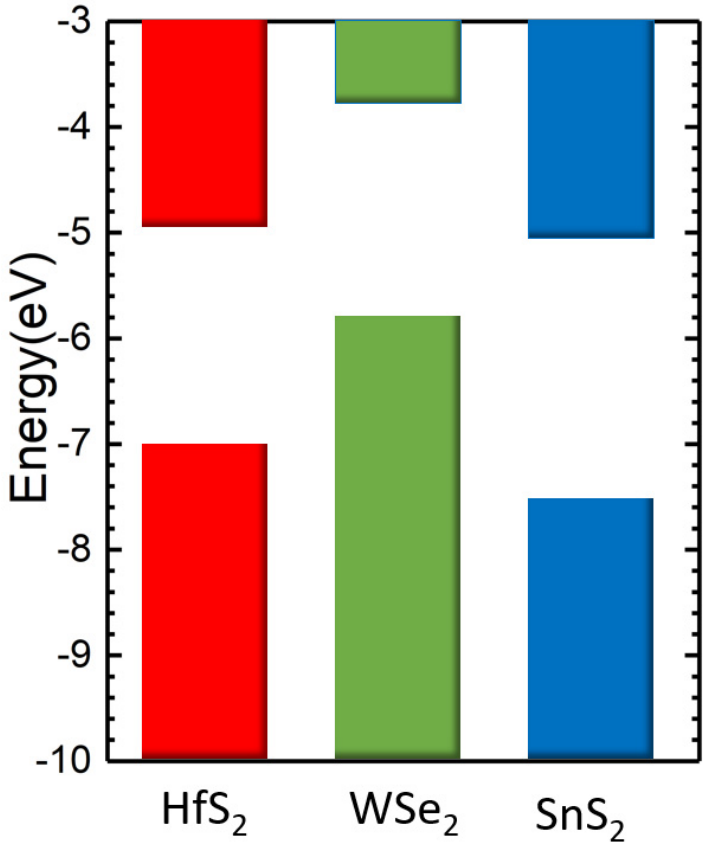

Fig. 3.

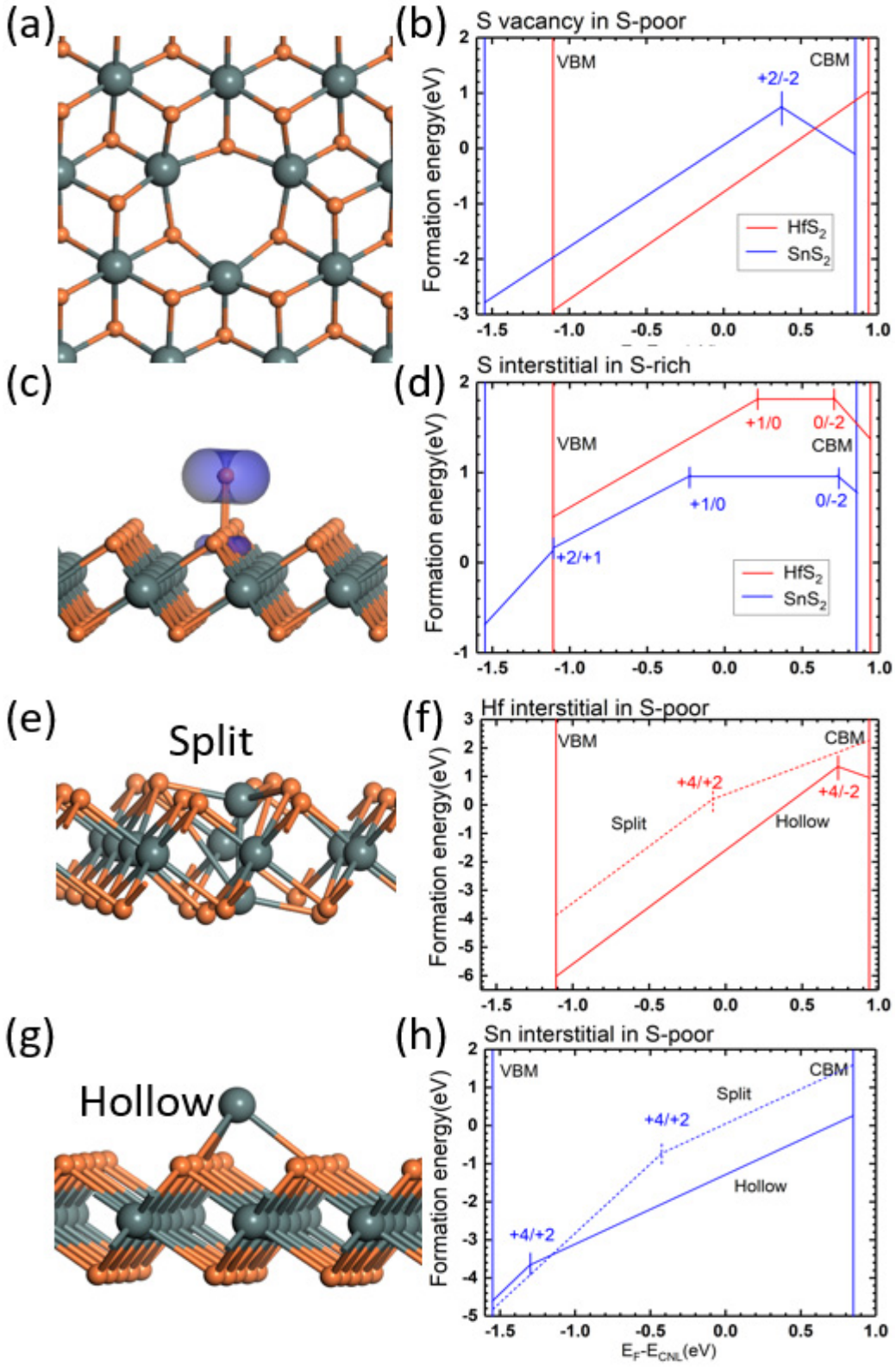
(a)
(b)
S vacancy in S-poor
VBM
CBM
+2/-2
Formation energy(eV)
HfS2
SnS2
(c)
(d)
S interstitial in S-rich
+1/0
0/-2
+2/+1
(e)
Split
(f)
Hf interstitial in S-poor
+4/+2
+4/-2
(g)
Hollow
(h)
Sn interstitial in S-poor
EF-ECNL(eV)

Fig. 4.

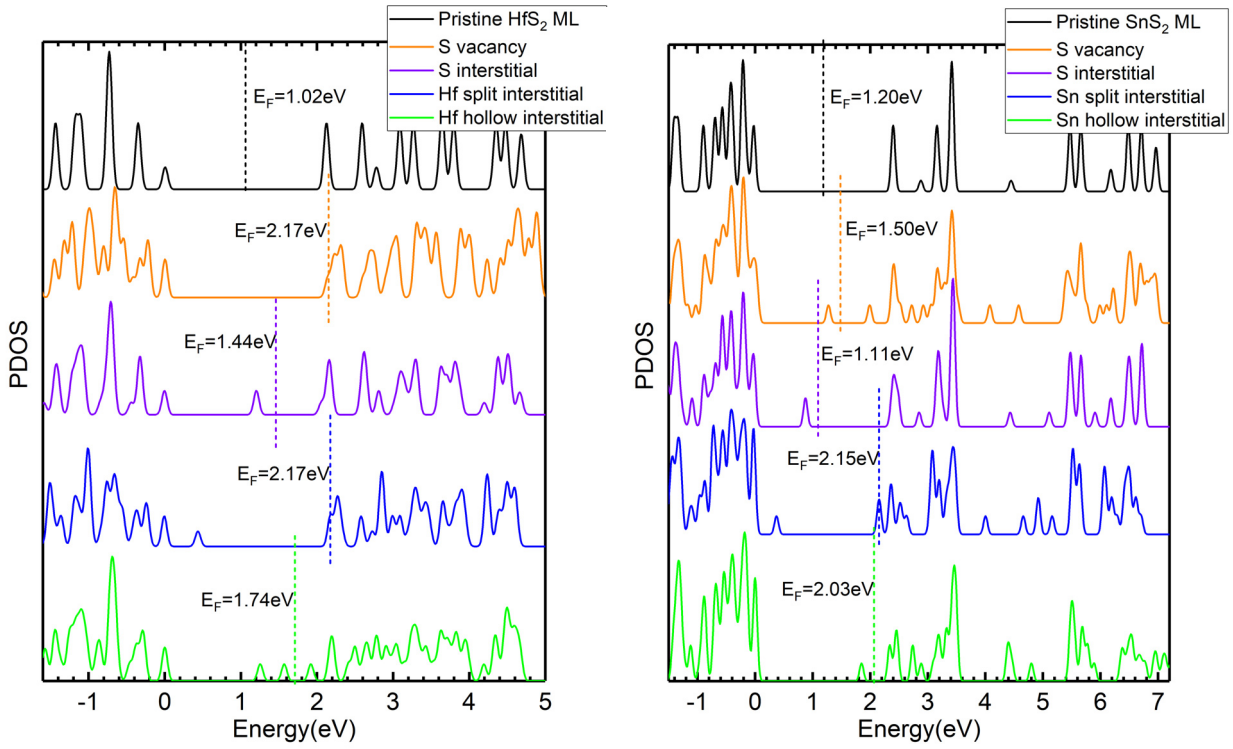
Pristine HfS2 ML
S vacancy
S interstitial
Hf split interstitial
Hf hollow interstitial
EF=1.02eV
EF=2.17eV
EF=1.44eV
EF=2.17eV
EF=1.74eV
PDOS
Energy(eV)
Pristine SnS2 ML
S vacancy
S interstitial
Sn split interstitial
Sn hollow interstitial
EF=1.20eV
EF=1.50eV
EF=1.11eV
EF=2.15eV
EF=2.03eV
PDOS
Energy(eV)

Fig. 5.

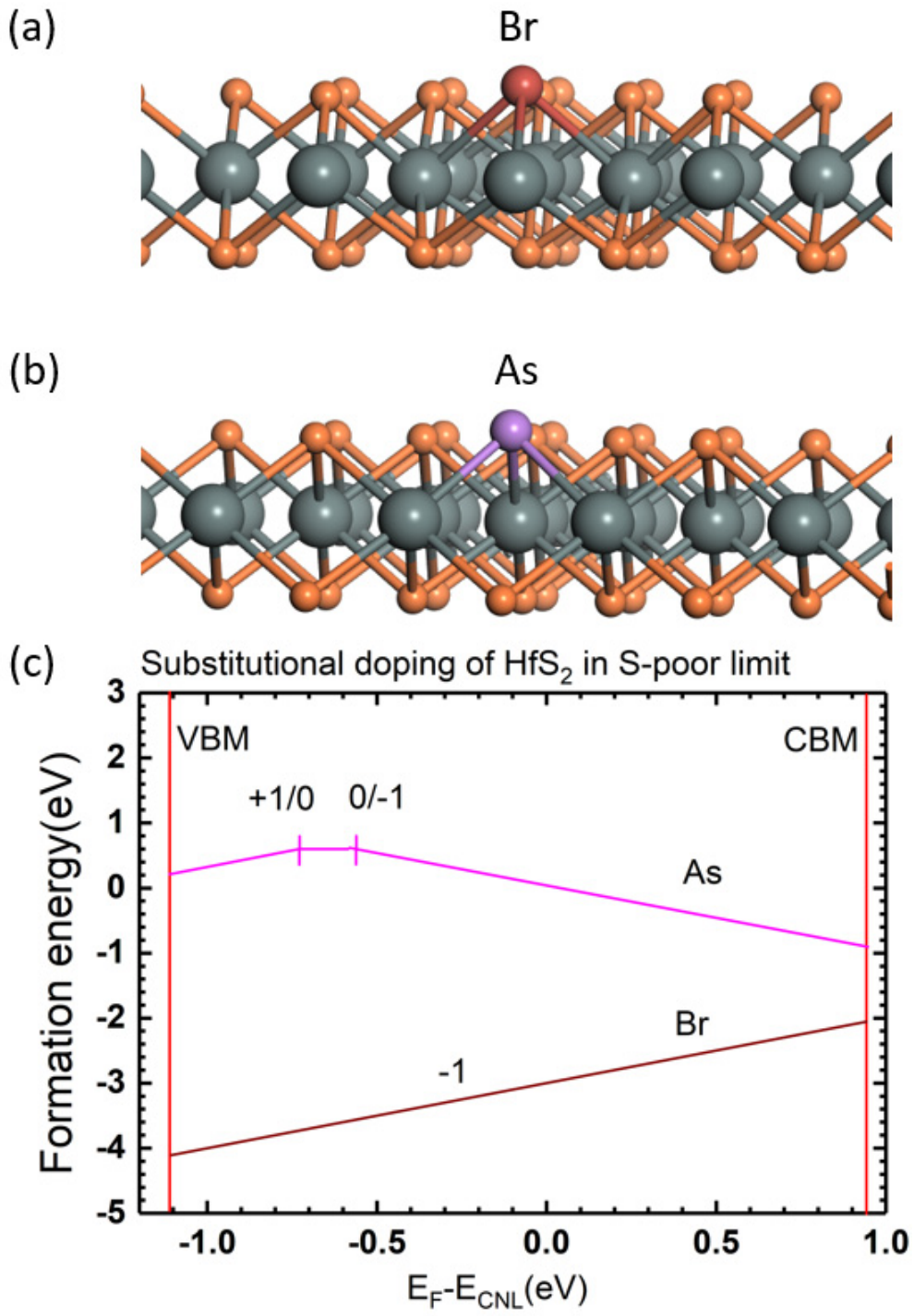
(a)
Br
(b)
As
(c)
Substitutional doping of HfS2 in S-poor limit
VBM
CBM
+1/0
0/-1
As
Br
-1
Formation energy(eV)
EF-ECNL(eV)
3
2
1
0
-1
-2
-3
-4
-5
-1.0
-0.5
0.0
0.5
1.0

Fig. 6.